Transformation of Nanocrystalline MgO Pellets in Reaction with 1-Chlorobutane

Piyush P. Gupta, Keith L. Hohn, and Larry E. Erickson
Dept. of Chemical Engineering, Kansas State University, Manhattan, KS 66506

Kenneth J. Klabunde and Alexander F. Bedilo
Dept. of Chemistry, Kansas State University, Manhattan, KS 66506

DOI 10.1002/aic.10229
Published online in Wiley InterScience (www.interscience.wiley.com).

Nanoscale MgO, prepared by an aerogel method (AP–MgO), has been found to be a good destructive adsorbent for dehydrochlorination of 1-chlorobutane. MgO is converted to $MgCl_2$ during reaction, but conversion continues because $MgCl_2$ itself is a good catalyst for dehydrochlorination. Pelletization will likely be required in industrial use of AP–MgO to ensure lower pressure drop. Pelletization, however, can lead to internal diffusion limitations. In addition, the phase transformation of MgO to $MgCl_2$ inside the pellets leads to physical changes that may limit the reaction rate. This study reports the changes in AP–MgO physical properties upon pelletization and reaction with 1-chlorobutane. Pore diffusion limitations are noted for all pellets. The phase transformation of MgO to $MgCl_2$ plays an important role in the process, as the physical characteristics substantially change with this transformation. A layer of $MgCl_2$ forms on top of MgO, rendering much of the starting pellet inaccessible to reactants. © 2004 American Institute of Chemical Engineers *AIChE J,* 50: 3195–3205, 2004

Keywords: adsorption, catalysis, porosity, nanoscale, pelletization, effectiveness factor, diffusion

Introduction

The nanoscale regime deals with the particles of 1 to 100 nm or about 10 to 10^6 atoms or molecules per particle (Klabunde, 1994). This regime represents a significant gap between the atomic scale represented by quantum chemistry and condensed matter represented by solid-state physics (Klabunde, 2001). It has been demonstrated that the size of nanoscale particles influences many physical and chemical properties (Vidal-Michel and Hohn, 2003; Wang and Herron, 1991). For example, the activity of gold particles is very sensitive to their size (Dai et al., 2003; Valden et al., 1998). With a decrease in the crystallite size of a material, more molecules are surface molecules rather than bulk molecules, which leads to an increased capacity for reaction (Kotz and Purcell, 1991). The large numbers of atoms located at the edges, corners, and surface of nanocrystallites provide many active sites for the reaction, and thus nanocrystalline materials often have enhanced reactivity (Carnes, 2000). Furthermore, on consolidating nanoscale particles into macroscale solids, the bulk material might exhibit new properties (Klabunde, 2001).

Heterogeneous catalysts tend to be sensitive to particle size in the nanoscale regime because the surface structure and the electronic properties can substantially change in this size range (Bell, 2003). Catalysis is largely dependent on active sites. Use of nanocrystalline materials makes it possible to modify the structure of the material and increase the concentration of active sites. This makes nanocrystalline materials very attractive for catalytic processes.

An objective of this research program is to develop destructive sorbents and catalysts that can be commercialized and used in air quality applications where chlorinated contaminants need

Correspondence concerning this article should be addressed to K. L. Hohn at hohn@ksu.edu.

to be treated. Finding sorbents and/or catalysts that are effective at room temperature would be ideal. The nanocrystalline MgO used in this work is a commercial product. More than 10 years of research and development have been carried out to reach the present state of development. The commercial production of nanocrystalline MgO has been a significant challenge because of the multiphase synthesis process that is needed and the byproducts that need to be managed in an environmentally efficient manner.

Nanocrystalline alkaline earth metal oxides, prepared by an aerogel technique, have been found to be very effective in treating halogenated hydrocarbons because of their adsorption capacity and reactivity (Klabunde et al., 1996a). The interaction of halogenated hydrocarbons with the surface of nanoparticles is referred to as destructive sorption, as both the surface and the bulk chemical composition of the oxides often change during the process (Klabunde et al., 1996b). Nanocrystals of metal oxides, including MgO, are particularly suitable for this reaction because the efficiency of the destructive sorption increases concomitantly with decreasing crystallite size of the metal oxide (Mishakov et al., 2002).

Prior research has shown that interaction of 1-chlorobutane (CB) with nanocrystalline AP–MgO at elevated temperatures results in both stoichiometric and catalytic dehydrochlorination of 1-chlorobutane to butene isomers. The reaction proceeds with the simultaneous conversion of MgO to $MgCl_2$ (Fenelonov et al., 2001). The interaction of 1-chlorobutane with MgO can be considered as a sum of destructive adsorption on the surfaces of the solid phase (Reaction 1) and the heterogeneous catalytic reaction on the surface of $MgCl_2$/MgO system (Reaction 2). The destructive reaction for the system can be expressed as

$$C_4H_9Cl \xrightarrow{MgO} C_4H_8 + HCl \qquad \text{and} \qquad MgO + 2HCl \rightarrow MgCl_2 + H_2O \quad (1)$$

The catalytic dechlorination part of the reaction can be expressed as

$$C_4H_9Cl \xrightarrow{MgCl_2} C_4H_8 + HCl \quad (2)$$

where $MgCl_2$ is the catalyst.

The conversion of MgO to $MgCl_2$ leads to changes in the textural properties of the solid phase. Complete conversion of nanoparticles of MgO to $MgCl_2$ should result in an increase in the volume of the solid phase by a factor of 3.64, as obtained by the Pilling–Bedworth (PD) equation (Fenelonov, 1994), expressed as follows

$$\nabla_{PB} = \frac{M_{MgCl_2}}{\rho_{MgCl_2}} \Big/ \frac{M_{MgO}}{\rho_{MgO}} \quad (3)$$

Although nanoscale materials appear to have outstanding properties as adsorbents and catalysts, questions remain about how to implement these materials. For use in a typical packed-bed reactor the powders of nanocrystals would need to be pelletized to avoid substantial pressure drop. However, pelletizing these powders may lead to internal diffusion limitations that would limit their effectiveness. This is particularly an issue in the hydrodechlorination reactions described above. The transformation of MgO to $MgCl_2$ may have profound effects on the structure of pelletized nanocrystals and, therefore, on pore diffusion limitations.

This work attempts to understand the effects of pelletization on the structure of nanocrystalline magnesium oxide and the effectiveness of using pellets of nanocrystalline magnesium oxide for the dehydrochlorination of 1-chlorobutane. The physical properties of powders and pellets of different sizes are probed before and after pelletization and before and after the dehydrochlorination reaction. Reaction rates are measured as functions of pellet size and the Thiele moduli of the pellets are calculated from the experimental data and from first principles.

Experimental

Pelletization of nanocrystalline AP–MgO powder

The AP–MgO used for the entire study was NanoActive Magnesium Oxide Plus™ (Nanoscale Materials Inc., Manhattan, KS). The material is guaranteed to have a surface area $>$ 600 m^2/g, with crystallite size of $<$4 nm and average pore diameter of about 30 Å. Tests in the laboratory showed that such assumptions are valid. This material has roughly the same physical and chemical properties as AP–MgO discussed by Fenelov et al. (2001) and Richards et al. (2000).

A fine powder of AP–MgO was compressed into tablet-shaped pellets using a manual hydraulic press (Fred S. Carver Inc., Gibbstown, NJ), capable of applying loads from 0 to 24,000 psi. The powder was placed in the standard IR pelletization die with a 12.9-mm-diameter cylindrical bore and the appropriate load was applied for a specific period of time. The load was ramped to the maximum studied load within 5 s. After the consolidation time, the entire load was removed at once.

No binder was used in making the pellets. AP–MgO powder was compressed at pressures of 10,000, 25,000, and 50,000 psi. The compression time for each load was varied from 15 to 60 s with an increment of 15 s. In each run 300 mg of AP–MgO powder was used for compression. The pellet obtained after the compression was checked visually for mechanical strength, as measured by its cohesiveness and firmness. Details about the pellet-making procedure can be found elsewhere (Gupta, 2003; Gupta et al. 2003a,b; Richards et al., 2000).

Physical characterization of powders and pellets

Surface adsorption studies were performed on mechanically firm pellets with a NOVA series 1200 gas sorption analyzer (Quantachrome Instruments, Boynton Beach, FL) using pure nitrogen (99.999%) as the adsorbate. Nitrogen adsorption isotherms at 77 K were used to characterize the pellets for BET surface area, total pore volume, pore size distribution, and average pore size. The Barett–Joyner–Halenda (BJH) method was used to obtain the pore size distribution from the equilibrium adsorption isotherm. A compete description of the method can be found in Satterfield (1991) and Vishwanathan et al. (2002).

X-ray diffraction studies were carried out using a Scintag XDS 2000 diffractometer. An X-ray gun emitting X-ray radi-

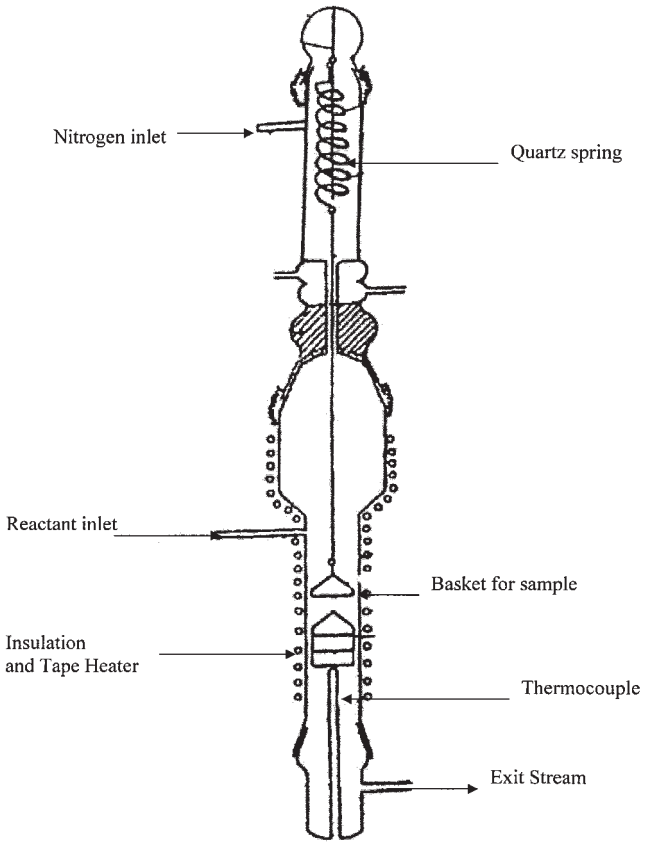

Figure 1. Experimental system used in the laboratory.

ation at 1.5418 Å was the radiation source. The sample was scanned between 20 and 80° with a speed of 2°/min. The width of the most intense diffraction peak (42° for MgO and 32.8° for $MgCl_2$) was used to estimate crystal sizes using the Scherrer equation (Niemantsverdriet, 2000).

Reaction of AP–MgO powder and pellets with 1-chlorobutane

The AP–MgO powder and the pellets, prepared using the procedures above, were used to catalyze dehydrochlorination of 1-chlorobutane. The rate of reaction and the mass of the powder or pellet were both measured as functions of time during dehydrochlorination.

To quantify the phase transformation from MgO to $MgCl_2$, the mass of the solid was continuously measured using a McBenn-type system. Displacement of a reference pointer in a quartz spring was used to measure the change in the mass of the sample as the reaction proceeds. A schematic of the apparatus is shown in Figure 1. Quantitative measurements of the concentration of 1-chlorobutane and butene were obtained using a gas chromatograph (model 580, Gow-Mac Instrument Co., Bethlehem, PA) with a Porapak P™ packed-bed column (Alltech Associates, Inc., Deerfield, IL) and thermal conductivity detector.

Before the reaction, each sample of AP–MgO powder or pellet was activated under flowing (5 L/h) nitrogen gas (99.9%, Airgas, Inc., Radnor, PA) at 500°C for 2 h to remove water and other chemisorbed compounds. The reaction was carried out at 350°C. Nitrogen was bubbled at 10 L/h through reagent-grade 1-chlorobutane (99.9%, Fisher Scientific, Pittsburgh, PA) at room temperature. Nitrogen was passed through the quartz spring section at a rate of 5 L/h. The resultant concentration of 1-chlorobutane, on mixing of the two streams, in the reaction zone was 4 mol %.

Pellets pressed at 25,000 psi and 30 s of compression were used for the reaction. Pellets were cylindrical in geometry and had a diameter of 12.9 mm. Pellets of three different weights were used and were characterized as small, medium, and large pellets for 100, 300, and 550 mg weight, respectively. A detailed description of the apparatus and procedures are given elsewhere in Gupta et al. (2003a), Gupta (2003), and Fenelonov et al. (2001).

Results and Discussion

Physical characterization of AP–MgO powder and pellets

It was observed that the most consistent and well-formed pellets with good mechanical strength were obtained with 25,000 psi load and 30 s of compression. It was observed that pellets compressed at 10,000 psi were not structurally firm and came apart easily. The pellets compressed at 50,000 psi were mechanically stable, but they tended to adhere to the die surface. Also it was observed that for times shorter than 30 s, the pellets were not mechanically stable and came apart easily. For excessive compression time, such as 45 or 60 s, they behaved like the 50,000 psi loading and adhered to the die surface. Based on the above observations, 30 s of loading was taken as the standard for comparing the performance of the pellets. AP–MgO powder was subjected to 10,000, 25,000, and 50,000 psi pressure and the pellets formed were characterized for their textural properties.

Nitrogen adsorption isotherms were analyzed for BET surface area, pore volume average pore radius, and void fraction inside the pellets. The results obtained are summarized in Table 1. Repeat trials for a particular compression strength were reproducible within 10–15%.

It is quite surprising to observe that surface area of the pellet formed after 10,000 psi compression has 904 m^2/g surface area, compared to 754 m^2/g surface area for AP–MgO powder. For medium and high compression, that is, at 25,000 and 50,000 psi, the pellets show a decrease in the surface area compared to 10,000 psi. This observation, although counterintuitive, is in good agreement with the results of Richards et al. (2000). They have also reported a very small increase, about 2–10%, in the surface area of the AP–MgO and AP–CaO when the powders are compressed into pellets at low compression. However, the

Table 1. Variation in the BET Surface Area, Pore Volume, Average Pore Radius, and Void Fraction of the Pellet with the Change in Consolidation Pressure

Sample	Surface Area (m^2/g)	Total Pore Volume (cm^3/g)	Average Pore Radius (Å)	Void Fraction
AP–MgO powder	754	0.49	13	0.64
Pellet–10,000 psi	904	0.65	14	0.70
Pellet–25,000 psi	803	0.59	15	0.68
Pellet–50,000 psi	651	0.55	17	0.67

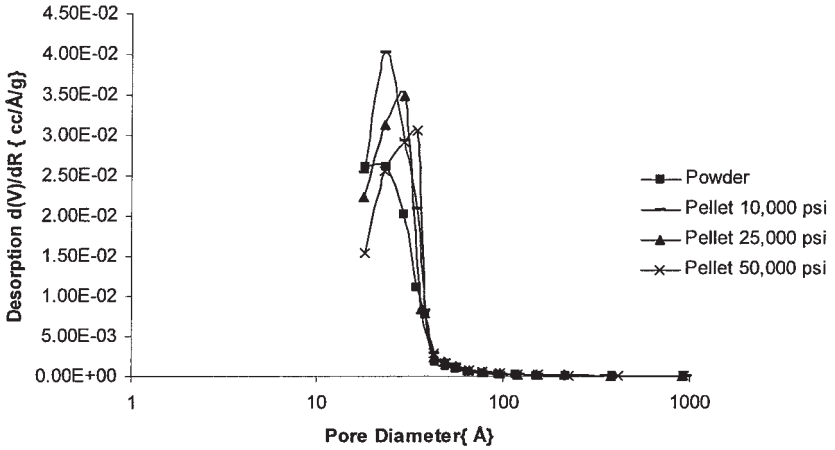

Figure 2. Pore-size distribution from the desorption isotherm of nitrogen on unreacted NanoActive-MgO in powder and pellet form with varying compressions.

observations in the present work show about 20% increase in the surface area for compression at 10,000 psi.

The increase in the surface area on mild compression can be attributed to the breaking of some aggregates or particles on application of pressure. This would naturally increase the surface area. However, on application of higher loads, some of the porous structure of the sample would collapse and cause a decrease in the surface area. This phenomenon reasonably explains the surface area change with the pressure applied. The result from this work also agrees with the work of Richards et al. (2000).

The results for the total pore volume show a trend similar to the surface area for the pellets. However, the values of total pore volume for all the pellet samples are observed to be greater than the value for powder. This could be explained by the volume that is external to the powder particles present in the pellets. There is consolidation of the pore volume at higher pressures. The average pore size has been calculated assuming a cylindrical pore geometry. The average pore size increases with increasing compression pressure.

The values of total pore volume and the true density of AP–MgO were used to determine porosity of the sample using the following equation

$$\varepsilon = \frac{V_{\text{Pore}}}{V_{\text{Pore}} + V'_{\text{Pellet}}} \tag{4}$$

where ε is void fraction, V_{Pore} is total pore volume per gram of the sample and V'_{Pellet} is the true volume occupied by 1 g of MgO in the pellet. Void fraction slightly decreases with increasing consolidation pressured, falling from 0.7 for 10,000 psi to 0.67 at 50,000 psi. The void fraction is lower for the powder than that for the pellet, which agrees with the trends noted for surface area and total pore volume.

A trend similar to that noted for average pore size radius is observed in the pore size distribution, as shown in Figure 2. From Figure 2 it can be observed that the local maxima for the plots have a rightward shift with increasing compression of the pellet. This shows that the most dominant pore size increases with increasing compression. This is in agreement with the calculation of the average pore size, as presented in Table 1.

Dehydrochlorination of 1-chlorobutane over AP–MgO powder and pellets

Experiments were carried out at three different concentrations of 1-chlorobutane in the reaction stream. The rate of reaction was found to be largely independent of the concentration of 1-chlorobutane. Analysis of the reaction results on a similar system studied by Fenelonov et al. (2001) has suggested that the reactions are zero order with respect to the concentration of 1-chlorobutane in the concentration range of the experiments. Thus the reaction rate, for both the stoichiometric and catalytic reactions, appears to be independent of the concentration of 1-chlorobutane at the conditions studied. This suggests that there were no external mass transfer limitations.

To study the effect of the reaction on the texture of AP–MgO and to study the effect of pelletization, 4 mol % of 1-chlorobutane in a nitrogen stream was used as a reactant. The rate of reaction was expressed as the rate of formation of butene (mmol min^{-1} g^{-1}). The rate of formation of butene in the given reaction system was the same as the rate of dehydrochlorination of 1-chlorobutane because no other products were ever detected. The weight of the powder and pellets, as used in the analysis, was the weight of the sample after the activation phase and before the reaction is started. The weight after activation of pellets in each category (that is, small, medium, or large pellet) was within 3% of 100, 300, and 550 mg, respectively. This range was ascribed to some material losses during pelletization and losses during activation stage.

The reaction rates for both powder AP–MgO and pelletized AP–MgO were normalized to obtain a meaningful comparison of the reaction rate per gram of starting AP–MgO. The reaction was carried out until the concentration of butene in the exit stream became constant (indicated by the area of the butene peak in the chromatogram). Some of the samples were studied until there was no butene formation. This indicated complete deactivation of both the stoichiometric and catalytic reactions. However, for the analysis and all the calculations herein, the maximum observed reaction rates were used. Plots of reaction rate vs. time for the reaction with powder, small pellet, medium pellet, and large pellet are shown in Figures 3a–d.

The effectiveness factors for the pellets were calculated by dividing the reaction rate for each pellet by that for powder

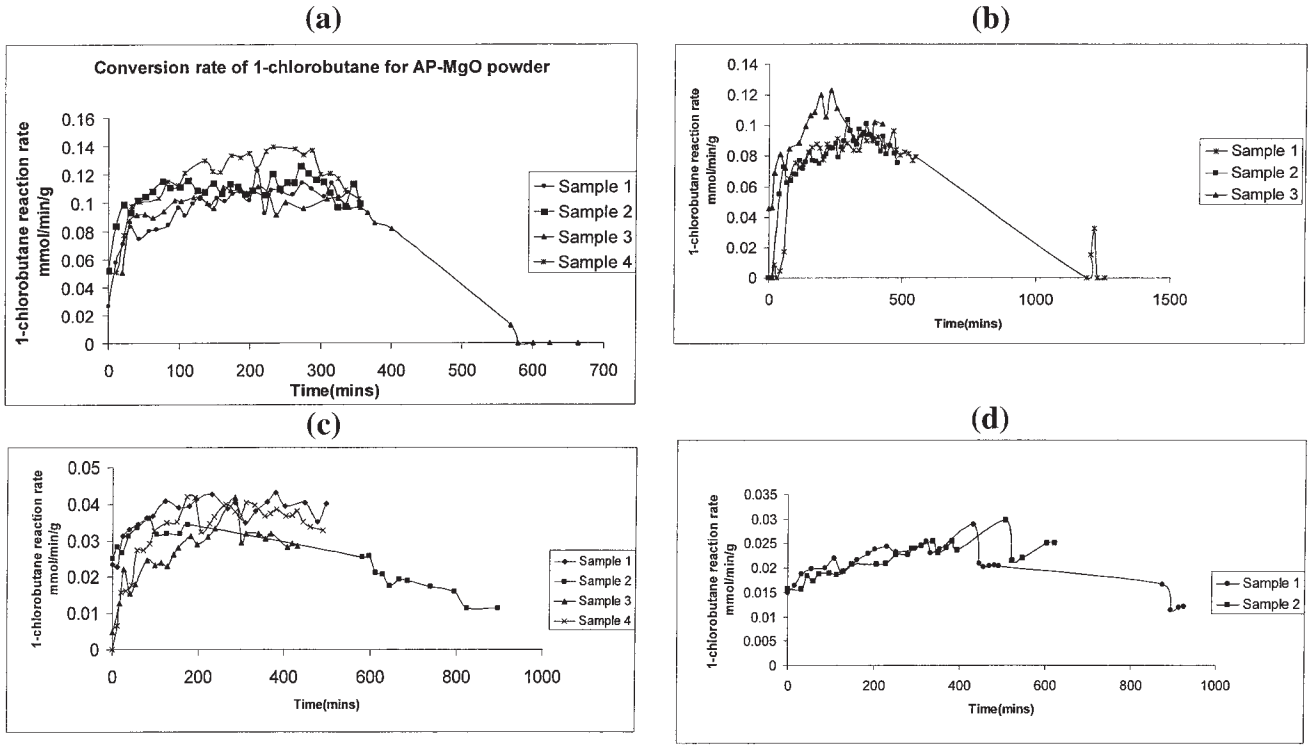

Figure 3. (a) Rate of conversion of 1-chlorobutane over NanoActive-MgO powder; (b) rate of conversion of 1-chlorobutane over NanoActive-MgO for a 0.1 g (small) pellet; (c) rate of conversion of 1-chlorobutane over NanoActive-MgO for a 0.3 g (medium) pellet; (d) rate of conversion of 1-chlorobutane over NanoActive-MgO for a 0.55 g (large) pellet.

AP–MgO, assuming that the powder reaction rate represents intrinsic kinetics without transport limitations. Thiele moduli were obtained assuming zero-order kinetics and using the standard chart for effectiveness factor vs. Thiele modulus as given in Fogler (1999). The Thiele modulus thus obtained is referred to as the *observed* Thiele modulus. The reaction rates, effectiveness factors, and observed Thiele moduli for reaction with AP–MgO in powder and pellets of different sizes are shown in Table 2. The values of Thiele modulus for a first-order reaction estimated from the same graph were not significantly different from the values for zero order. Because the Thiele modulus values are quite large for pellets of 0.3 and 0.55 g, this suggests significant diffusion limitation in the pellet.

The percentage conversion of MgO to $MgCl_2$ (α) was calculated using the initial and final weights of the pellet or powder. The weight of any carbonaceous deposits on the catalysts was ignored. Although most samples had some accumulated carbonaceous deposits on the surface of the pellet, the weight of the deposits was 2% or less of the total powder or pellet weight. It is believed that the deposits were polymerized butylenes and other sorbed products, not elemental carbon, because of the low temperature of reaction. Details of how α was calculated are given in Appendix B.

Table 2. Reaction Rate Expressed per Gram MgO, Effectiveness Factor, and Thiele Moduli for AP–MgO Powder and Pellets

Sample	Reaction Rate (mmol min^{-1} g^{-1})	Effectiveness Factor	Thiele Modulus
Powder	0.12	1	
0.1 g pellet	0.09	0.75	5
0.3 g pellet	0.035	0.3	19
0.55 g pellet	0.025	0.2	31

The percentage conversion values of MgO to $MgCl_2$ for the powder and all pellets are shown as functions of time in Figure 4. Figure 4 shows that for the larger pellets the conversion of MgO to $MgCl_2$ continues to increase with time, although 1-chlorobutane conversion plots show a steady state at an earlier time. This may be a result of the simultaneous conversion of MgO to $MgCl_2$ and decrease in $MgCl_2$ catalytic activity attributed to a decrease in surface area or deposition of carbonaceous deposits on the sample. This hypothesis is supported by the fact that in two cases when the reaction was carried out for up to 14 h, complete deactivation of the reaction system, characterized by no detectable butene formation, was observed. This effect can be observed for sample 3 in Figure 3a, and sample 1 in Figure 3b.

Because the amount of $MgCl_2$ present in a sample plays an important role in the rate of catalytic reaction, it might be better to express the reaction rate as the rate of dehydrochlorination of 1-chlorobutane per unit mass of $MgCl_2$, compared to the rate expressed per unit mass of starting MgO. The values of reaction rate given in Table 2 can be converted to reaction rate per unit mass of $MgCl_2$ in the reaction, using values of percentage conversion of MgO into $MgCl_2$. The rate of dehydrochlorination of 1-chlorobutane per unit mass of $MgCl_2$ in the sample after the reaction can be calculated using the equation as given in Appendix C. The effectiveness factor for this reaction rate

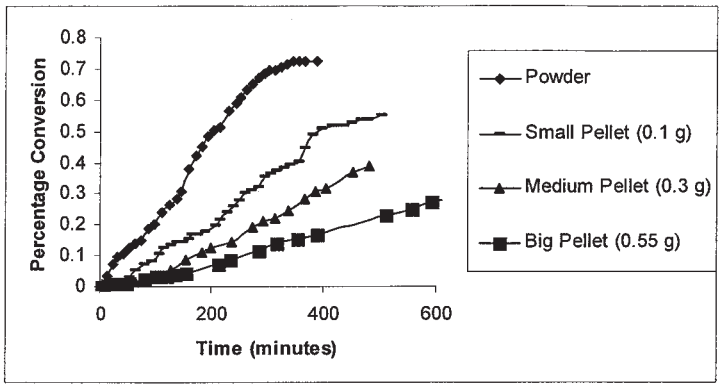

Figure 4. Percentage conversion of MgO to $MgCl_2$ vs. reaction time for powder and pellets.

and the observed Thiele modulus for the reaction rate per gram of $MgCl_2$ were obtained as before. The values of reaction rate per gram of $MgCl_2$ and corresponding effectiveness factor and Thiele modulus are given in Table 3.

As seen in Table 3, the reaction rate for the 0.1 g pellet is in fact slightly higher than that for the powder, leading to an effectiveness factor of 1. The reaction rates for the 0.3 g pellet and the 0.55 g pellet are also almost the same. The effectiveness factors for the 0.3 g pellet and the 0.55 g pellet are 0.58 and 0.56, respectively. This analysis gives a Thiele modulus of 8 for the 0.3 g pellet and 7 for the 0.55 g pellet. The Thiele modulus for the 0.1 g pellet was not calculated because the value of its effectiveness factor is almost 1. The results presented in Table 3 indicate that there is some diffusion limitation for reaction with medium and large pellets when the reaction rate is expressed as moles of 1-chlorobutane converted per gram of $MgCl_2$ formed in the sample during the reaction.

The trends in the effectiveness factors when the rate was expressed per gram MgO were different from those when the reaction rate was expressed per gram $MgCl_2$. When expressed per gram of MgO, all pellets exhibited some pore diffusion limitations. Pore diffusion limitations were extensive for the largest two pellets. When the reaction rate was expressed per gram $MgCl_2$, on the other hand, there were no apparent pore diffusion limitations for the 0.1 g pellet, and the effectiveness factors for the 0.3 and 0.5 g pellets were larger than those when MgO was used as the basis.

The likely explanation for these trends is that much of the MgO surface area of the pellets is not used because of pore diffusion limitations. The reactant 1-chlorobutane does not reach the innermost portions of the pellet. This means a decreased reaction rate compared to that of the powder (effectiveness factor < 1). Furthermore, because 1-chlorobutane does not diffuse through all parts of the pellet, MgO is converted to $MgCl_2$ only near the surface of the pellet. The $MgCl_2$ layer may also act to obstruct pores, further preventing diffusion inside the pellet. However, this layer is available for the catalytic hydrodechlorination because it is near the surface of the pellet. This leads to an effectiveness factor near one for the smallest pellet, and larger effectiveness factors than on an MgO basis for the other two pellets.

The Thiele modulus for the dehydrochlorination reaction can also be derived numerically using the definition in the following equation. The value of Thiele modulus, thus obtained, can be compared to the previous Thiele moduli obtained experimentally

$$\phi_s^2 = \frac{r_p^2(-r')}{D_{eff}C_s} \tag{5}$$

where ϕ_s is the Thiele modulus, r_p is the characteristic length for pellet (thickness of pellet/2), r' is the rate of reaction for pellet (moles/volume of pellet/time), D_{eff} is the effective diffusivity for the limiting reactant, and C_s is the concentration of the limiting reactant (moles/volume). A complete analysis of Eq. 5 and methodology to obtain the Thiele modulus is found in Appendix D. The values of void fraction, effective diffusivity, and Thiele modulus for NanoActive-MgO pellets are shown in Table 4.

The values of calculated Thiele moduli are lower than the corresponding values of observed Thiele moduli by a factor varying from 2.5 to 5. This difference may be attributable to the estimate of the effective diffusivity used to calculate the Thiele modulus. Over time there are substantial changes in the surface area and void fraction of each sample, as described below, resulting from the formation of $MgCl_2$ and sintering of parti-

Table 3. Reaction Rate Expressed per Gram of $MgCl_2$, Effectiveness Factor, and Thiele Moduli for AP–MgO Powder and Pellets

Sample	Reaction Rate (mmol min^{-1} g^{-1})	Effectiveness Factor	Thiele Modulus
Powder	0.0685		
Pellet			
0.1 g	0.0694	1.01	NA
0.3 g	0.0394	0.58	8
0.55 g	0.0386	0.56	7

Table 4. Values of Void Fraction, Effective Diffusivity, and Calculated Thiele Moduli for the Catalytic Reaction for Different Size Pellets

Sample	Void Fraction	Effective Diffusivity (m^2/s)	Thiele Modulus
0.1 g pellet	0.11	5.85E-08	2.08
0.3 g pellet	0.14	9.36E-08	4.81
0.55 g pellet	0.21	2.21E-07	5.95

Table 5. Nitrogen Physisorption Data for AP–MgO Powder before the Reaction and Powder and Pellets after the Reaction

Sample	BET Surface Area (m^2/g)	Total Pore Volume (cm^3/g)	Avg. Pore Radius (nm)
Initial powder	754 ± 56	0.49 ± 0.11	1.3 ± 0.2
After reaction powder	22 ± 8	0.026 ± 0.01	9.0 ± 2.8
After reaction small pellet (0.1 g)	9 ± 5.3	0.043 ± 0.025	9.8 ± 1.7
After reaction medium pellet (0.3 g)	15 ± 6.7	0.052 ± 0.02	6.7 ± 1.1
After reaction big pellet (0.55 g)	16 ± 0.48	0.083 ± 0.02	8.1 ± 2.8

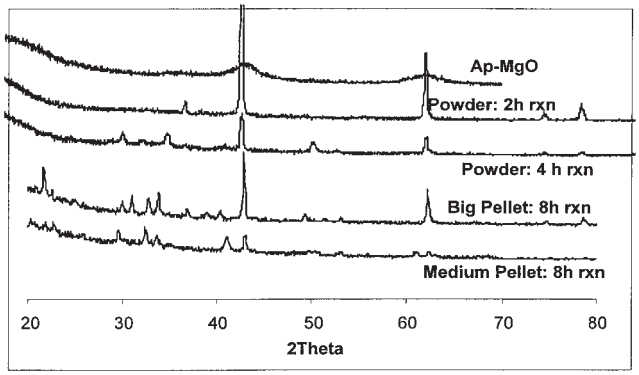

Figure 5. XRD diffractograms for samples before and after reaction.

cles. The actual effective diffusivities, therefore, may be lower than those used to estimate the Thiele moduli that relied on the initial properties of the pellets to calculate effective diffusivity.

The Thiele modulus for the stoichiometric reaction can also be estimated using analysis similar to the catalytic phase of the reaction. The Thiele modulus for the stoichiometric phase can be calculated for times very close to the start of the reaction. At those times, it can be safely assumed that the reaction would be predominantly stoichiometric and the pellet would have retained its original pore structure. The reaction rate for NanoActive-MgO powder at 15 min was 0.02 mmol min^{-1} g^{-1}. The pore volume of the pellets can safely be assumed to be equal to the pore volume before the start of the reaction. Thus the pore volume for pellets, from Table 1, is 0.59 cm^3/g. The concentration of 1-chlorobutane is 1 vol % in nitrogen. The effective diffusivity is similar to the diffusivity for the catalytic phase. The bulk density of NanoActive-MgO pellets is 1000 kg/m^3. Using these values, the Thiele moduli for the small, medium, and large pellets were calculated to be 0.14, 0.4, and 0.73, respectively. These values are much less than those calculated for the catalytic reaction, and they suggest no diffusion limitation in the pellets during the stoichiometric reaction.

The surface area, pore volume and the average pore diameter were measured for the starting powder and the powder and pellets after the reaction using nitrogen adsorption. These results are presented as Table 5. As seen in this table, there is a significant decrease in the surface area of the powder and pelletized material during reaction. The surface area and total pore volume both decrease by over an order of magnitude. This may be explained by the textural changes brought about by the conversion of MgO to $MgCl_2$. Specifically, $MgCl_2$ may block some of the micropores. This phenomenon is supported by scanning electron microscopy (SEM) images discussed below.

The surface area and pore volume are smallest for the small pellet. The surface area for the powder after reaction is larger than even the largest pellet. This could be attributable to sintering of the porous material inside the pellets associated with the reaction. Sintering would be less in powder formed of loose porous aggregates.

The average pore radius for the samples after the reaction is very large compared to the values before the reaction. The trend is similar to the effect of pellet size on the surface area after the reaction, albeit in reverse order. The average pore radius for small pellets (0.1 g) after the reaction is higher compared to the pore radius for powder after the reaction. However, among the pellets, the pore radius decreases as the size of the pellet increases.

The X-ray diffraction patterns were obtained for all samples before and after reaction to probe the changes in the crystalline phases. These are shown in Figure 5. Initially only very small MgO crystallites exist, as shown by the two broad peaks at 42 and 62°. During reaction, those two peaks become much sharper, indicating an increase in crystallite size. Additional peaks appear in the diffraction pattern at 30.3 and 32.8°, indicating that $MgCl_2$ is present.

The size of the crystalline phase was calculated using the Scherrer equation and the values are given in Table 6. As seen in this table, the MgO crystallite size increases from 6.1 nm before the reaction to 33.8 nm after the reaction. This can be easily seen from the narrowing of the peak in NanoActive-MgO powder and pellet samples after the reaction. The crystallite size data for MgO do not show a definite trend while going from powder to pellets. However, as in the surface area and pore volume results, the crystallite size of medium pellet is lower compared to the crystallite size of the powder after the reaction, but higher than that of the large pellet. The crystallite size of $MgCl_2$, on the other hand, increases from the powder to medium pellet to large pellet, although the degree of conversion of MgO to $MgCl_2$ was in the reverse order.

SEM analysis was used to observe the microstructure of the samples before and after the reaction. The images obtained are shown as Figures 6a–c. The images clearly show the degradation of the ordered structure in NanoActive-MgO as the reaction proceeds. The ordered and crystalline structure of NanoActive-MgO becomes less ordered with reaction time. The pores, easily seen in the NanoActive-MgO sample before the reaction, start disappearing as the reaction proceeds. An amorphous disordered layer appears on the MgO structure as the reaction proceeds. This coating of $MgCl_2$ may be responsible

Table 6. Crystallite Sizes of Powders and Pellets before and after Reaction

Sample	MgO Crystallite Size (nm)	$MgCl_2$ Crystallite Size (nm)
Powder before reaction	6.1	NA
Powder after reaction	33.8	18.1
0.3 g pellet after reaction	26.5	23.9
0.55 g pellet after reaction	41.3	27.2

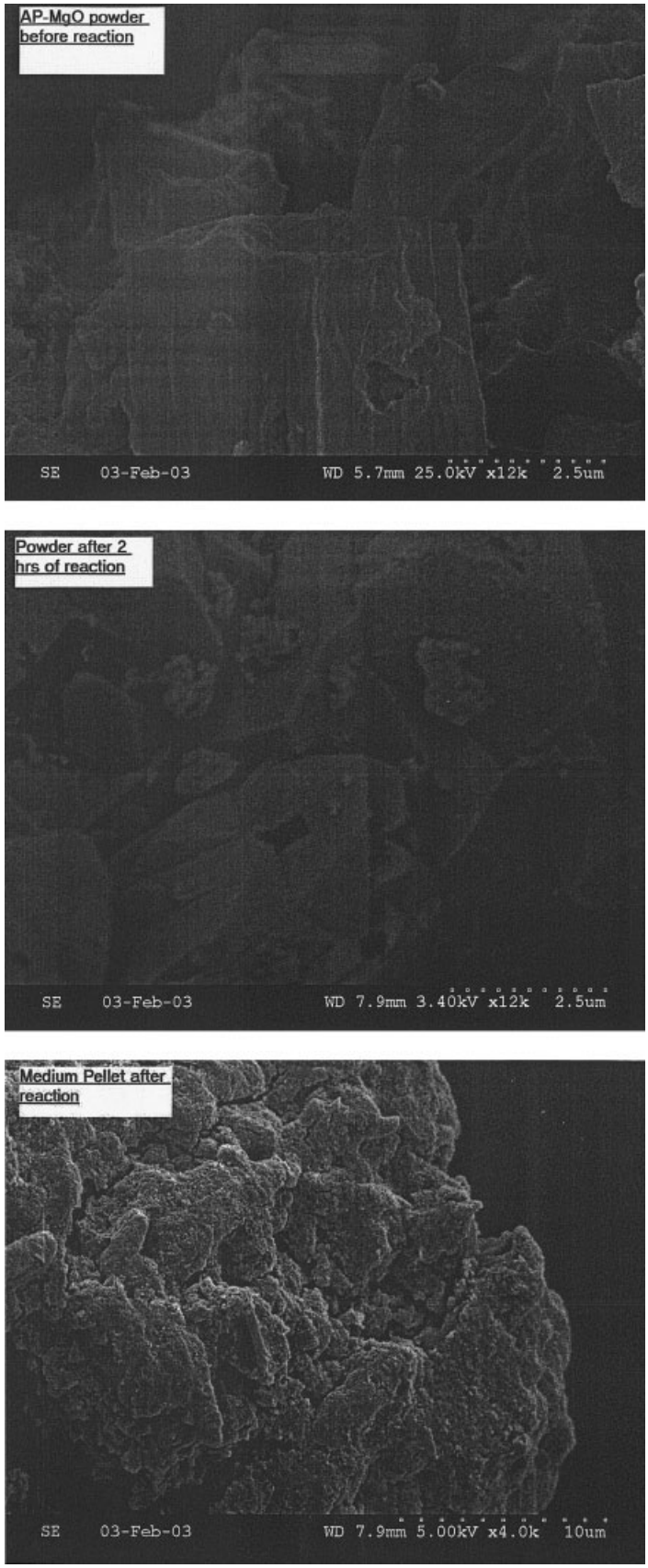

Figure 6. (a) SEM image of NanoActive-MgO powder before reaction; (b) SEM image of reacted powder after 2 h of reaction; (c) SEM image of reacted pellet after 8 h of reaction.

for the less-ordered structure and the blocking of the pores in the sample, and might explain the significant decrease in the surface area and pore volume of the catalytic material as the reaction proceeds.

From the Pilling–Bedworth equation (Eq. 3), it can be argued that an increase in the volume of the solid phase may result in the formation of a coating of $MgCl_2$ over unreacted particles of MgO. This might possibly lead to blockage or reduced access to the micropores in the material. Fenelonov et al. (2001) discuss that theoretically the surface area of the sample should not change appreciably with the reaction and the subsequent conversion of MgO into $MgCl_2$ unless there is sintering of the particles. However, it is observed that there is a significant decrease in the surface area with reaction time. There was no increase in the volume of the sample and thus the specific area decrease can be attributed to the aggregation of the primary particles with growth of their size.

From the data presented above, it can be established that the conversion of MgO to $MgCl_2$ decreases with the increase in the initial size of the pellet. This could be a result of the inability of 1-chlorobutane to reach the MgO in the inner parts of the pellet. Blocking of pores in the sample can prevent the reactants from reaching the inner parts of the pellet, and thus the destructive adsorption and conversion of MgO to $MgCl_2$ are restricted. This would also limit the transport of 1-chlorobutane to the inner parts of the pellets and thus the low conversion ascribed to destructive adsorption.

Both the stoichiometric and catalytic reaction rates depend on the surface area of NanoActive-MgO powder or pellet available during the reaction. The surface area of powder or pellet decreases with the extent of reaction. Because the stoichiometric reaction occurs before the catalytic reaction, the surface area available for reaction during the stoichiometric reaction phase may be substantially more than the surface area available during the catalytic reaction phase. The lower availability of surface area during the catalytic reaction phase reduces the reaction rate. For larger pellets, the conversion to $MgCl_2$ is lower compared to that of powder and smaller pellets. Thus the extent of catalysis, per unit mass of starting MgO, would be lower. This would lead to a lower reaction rate for conversion of 1-chlorobutane or formation of butene. The transport limitation attributed to the effect of diffusion would also limit the reaction rate. The combined effects of the above factors contribute to the high Thiele modulus values observed for 0.3 and 0.55 g pellets.

Conclusions

The destructive sorption of 1-chlorobutane on MgO led to significant structural changes in all samples. Surface area and pore volumes decreased dramatically, whereas the average pore radius increased. In addition, the ordered MgO structure became highly disordered. These results were primarily caused by the conversion of MgO to $MgCl_2$. $MgCl_2$ has a higher specific volume than that of MgO, so as it is created it blocks some of the porous network. Sintering and aggregation of crystallites/particles of AP–MgO inside the pellet also may have played a role in the observed physical changes.

It has been found that there were substantial pore diffusion limitations in the pellets, especially for the largest two pellets. Because of the pore diffusion limitations, 1-chlorobutane was unable to diffuse all the way into the pellets and therefore MgO is not converted into $MgCl_2$ everywhere in the pellet. This effect may have been exacerbated by the fact that when $MgCl_2$ was formed it blocked the pores that penetrate deeper into the pellet. The structural characterization and SEM micrographs suggest that the outer portions of the pellets were converted to $MgCl_2$, resulting in a pellet with a layer of $MgCl_2$ on the outside of a layer of MgO. The MgO layer in the interior portion of the pellet did not contribute to the reaction rate because it was inaccessible to 1-chlorobutane as a result of blocked pores and severe pore diffusion limitations.

Literature Cited

Bell, A. T., "The Impact of Nanoscience on Heterogeneous Catalysis," *Science*, **299**, 1688 (2003).

Bird, R. B., W. E. Stewart, and E. N. Lightfoot, *Transport Phenomena*, Wiley, New York (1960).

Carnes, C. L., "The Chemical and Catalytic Properties of Nanocrystalline Metal Oxides Prepared Through Modified Sol–Gel Synthesis," PhD Thesis, Kansas State University, Manhattan (2000).

Dai, S., B. Lee, H. Zhu, Z. Zhang, and S. H. Overbury, "Controlled Preparation of Gold-Nanoparticle Catalysts in Porous Materials: Synergistic Interplay of Self-Assembly, Nucleation, and Topology," Proc. of 18th NAM, Cancun, Mexico, June (2003).

Fenelonov, V., M. S. Mel'gunov, I. V. Mishakov, R. M. Richards, A. M. Volodin, and K. J. Klabunde, "Changes in Texture and Catalytic Activity of Nanocrystalline MgO during its Transformation to $MgCl_2$ in the Reaction with 1-Chlorobutane," *J. Phys. Chem. B*, **105**, 3937 (2001).

Fenelonov, V. B., "Change of Texture upon Topochemical Transformations," *React. Kinet. Catal. Lett.*, **52**, 367 (1994).

Fogler, H. S., *Elements of Chemical Reaction Engineering*, 3rd Edition, Prentice Hall, Upper Saddle River, NJ (1999).

Gupta, P. P., "Effect of Pelletization on Chemical Activity, Textural Properties and Structure of Aerogel Prepared Nanocrystalline Magnesium Oxide in Reaction with 1-Chlorobutane," MS Thesis, Kansas State University, Manhattan (2003).

Gupta, P. P., A. F. Bedilo, K. J. Klabunde, and L. E. Erickson, "Effect of Diffusion and Textural Changes on the Catalytic Activity and Adsorption of Nanocrystalline MgO Pellets in Reaction with 1-Chlorobutane," Proc. of 18th North American Catalysis Society Annual Meeting, Cancun, Mexico (2003b).

Gupta, P. P., K. L. Hohn, K. J. Klabunde, and L. E. Erickson, "Evaluating Changes in Catalytic Activity and Adsorption of Nanocrystalline MgO in Reaction with 1-Chlorobutane with Reaction Time and Compression to Pellets," Proc. of AIChE Annual Conf., San Francisco, November (2003a).

Heinrichs, B., J. P. Pirard, and J. P. Schoebrechts, "Mass Transfer in Low Density Xerogel Catalysts," *AIChE J.*, **47**, 1866 (2001).

Klabunde, K. J., *Free Atoms, Clusters and Nanoscale Particles*, Academic Press, San Diego, CA (1994).

Klabunde, K. J., *Nanoscale Materials in Chemistry*, Wiley, New York (2001).

Klabunde, K. J., D. G. Park, J. V. Stark, O. Koper, S. Decker, Y. Jiang, and I. Lagadic, "Nanoscale Metal Oxides as Destructive Adsorbents. New Surface Chemistry and Environmental Applications," *Fine Particles Science and Technology*, E. Pelizzetti, ed., Kluwer Academic, Dordrecht, The Netherlands, pp. 691–706 (1996).

Klabunde, K. J., J. Stark, O. Koper, C. Mohs, D. G. Park, S. Decker, Y. Jian, I. Lagadic, and D. Zhang, "Nanocrystals as Stoichiometric Reagents with Unique Surface Chemistry," *J. Phys. Chem.*, **100**, 12142 (1996).

Kotz, J., and K. F. Purcell, *Chemistry and Chemical Reactivity*, 2nd Edition, Saunders College Publishing, London (1991).

Mishakov, I. V., A. F. Bedilo, R. M. Richard, V. V., Chesnokov, A. M. Volodin, V. I. Zaikovskii, R. A. Buyanov, and K. J. Klabunde, "Nanocrystalline MgO as a Dehydrohalogenation Catalyst," *J. Catal.*, **206**, 40 (2002).

Niemantsverdriet, J. W., *Spectroscopy in Catalysis*, 2nd Edition, Wiley–VCH, Weinheim, Germany (2000).

Richards, R., W. Li, S. Decker, C. Davidson, O. Koper, V. Zaikovski, A.

Volodin, T. Rieker, and K. J. Klabunde, "Consolidation of Metal Oxide Nanocrystals. Reactive Pellets with Controllable Pore Structure that Represents a New Family of Porous Inorganic Materials," *J. Am. Chem. Soc.*, **122**, 4921 (2000).
Satterfield, C. N, *Heterogeneous Catalysis in Industrial Practice*, 2nd Edition, McGraw Hill, New York (1991).
Valden, M., X. Lai, and D. W. Goodman, "Onset of Catalytic Activity of Gold Clusters on Titania with the Appearance of Nonmetallic Properties," *Science*, **281**, 1647 (1998).
Vidal-Michel, R., and K. L. Hohn, "Effect of Crystal Size on the Oxidative Dehydrogenation of Butane," *J. Catal.*, **221**, 127 (2003).
Vishwanathan, B., S. Sivasanker, and A. V. Ramaswamy, *Catalysis: Principles and Application*, Narosa Publishing House, New Delhi (2002).
Wang, Y., and N. Herron, "Nanometer-sized Semiconductor Clusters. Materials Synthesis, Quantum Size Effects, and Photophysical Properties," *J Phys. Chem.*, **95**, 525 (1991).

Appendix

A. Void fraction calculation

$$\varepsilon = \frac{V_{\text{Pore}}}{V_{\text{Pore}} + V'_{\text{Pellet}}} \tag{A1}$$

where ε is the void fraction; V_{Pore} is the total pore volume per gram of the sample; and V'_{Pellet}, which is the true volume occupied by 1 g of MgO in the pellet, can be calculated using the following relation

$$V'_{\text{Pellet}} = \frac{1}{\rho_{\text{MgO}}} \tag{A2}$$

where

ρ_{MgO} is the true density of MgO (3.65 gm/cm^3).

B. Percentage conversion of MgO to $MgCl_2$

$$w_f = w_i\left[(1-\alpha) + \alpha\left(\frac{M_{\text{MgCl}_2}}{M_{\text{MgO}}}\right)\right] \tag{B1}$$

where α is the percentage conversion of the sample, w_f is the final weight of the sample, w_i is the initial weight of the sample, M_{MgCl_2} is the molecular weight of $MgCl_2$, and M_{MgO} is the molecular weight of MgO.

C. Conversion of reaction rate to reaction rate expressed per gram of $MgCl_2$

$$R_2 = \frac{R_1}{\alpha\left(\frac{M_{\text{MgCl}_2}}{M_{\text{MgO}}}\right)} \tag{C1}$$

where R_1 is the reaction rate per gram of MgO at the start of the reaction, R_2 is the reaction rate per gram of $MgCl_2$ in the sample after the reaction, M_A is the molecular weight of compound A, and α is the fractional conversion of MgO to $MgCl_2$.

D. Calculating Thiele modulus

According to the definition, the Thiele modulus can be expressed as follows

$$\phi_s^2 = \frac{r_p^2(-r')}{D_{eff}C_s} \tag{D1}$$

where, ϕ_s is the Thiele modulus, r_p is the characteristic length for pellet (thickness of pellet/2), r' is the rate of reaction for pellet (moles/volume of pellet/time), D_{eff} is the effective diffusivity for the limiting reactant, and C_s is the concentration of the limiting reactant (moles/volume).

The equation can be rewritten as

$$\phi_s^2 = \frac{r_p^2(-r)\rho}{D_{eff}C_s} \tag{D2}$$

where r is the rate of reaction for pellet (moles/mass of pellet/time) and ρ is the bulk density of the catalyst pellet.

The value of C_s can be obtained using the following

$$C_s = \frac{P_{\text{CB}}x}{RT} \tag{D3}$$

where P_{CB} is the partial pressure of 1-chlorobutane in inlet stream (0.04 atm), x is the fractional conversion of 1-chlorobutane obtained (0.5), R is the universal gas constant (0.0821 atm/mol/K), and T is the temperature (K).

D_{eff} can be calculated using the following relation, described in Heinrichs et al. (2001) and Satterfield (1991)

$$\frac{1}{D_{eff}} = \frac{\frac{1}{D_m} + \frac{1}{0.097R_0\sqrt{\frac{T}{M}}}}{\varepsilon_p^2} \tag{D4}$$

where D_{eff} is the effective diffusivity (m^2/s), D_m is the bulk diffusivity (m^2/s), R_0 is the pore radius (m), T is the temperature (K), M is the molecular weight of 1-chlorobutane (kg/mmol), and ε_p is the void fraction.

The value of D_m was obtained as 4.5×10^{-5} m^2/s for the reaction at 350°C (623 K) using the Chapman–Enskog equation (Bird et al., 1960). The void fraction can be calculated by modifying Eqs. A1 and A2 to account for the change in true volume occupied by MgO and $MgCl_2$ in the pellet. Thus,

$$V'_{\text{Pellet}} = (1-\alpha)V'_{\text{MgO}} + \alpha V'_{\text{MgCl}_2} \tag{D5}$$

where V'_{Pellet} is the true volume occupied by MgO and $MgCl_2$ per gram of pellet, α is the fractional conversion of MgO to $MgCl_2$ (from values in Figure 4), V'_{MgO} is the true volume occupied by MgO per gram of pellet, and V'_{MgCl_2} is the true volume occupied by $MgCl_2$ per gram of pellet.

Also,

$$V'_{\text{MgO}} = \frac{1}{\rho_{\text{MgO}}} \tag{D6a}$$

$$V'_{\text{MgCl}_2} = \frac{1}{\rho_{\text{MgCl}_2}} \tag{D6b}$$

where ρ_{MgO} is the true density of MgO (3.65 g/cm^3) and ρ_{MgCl_2} is the true density of $MgCl_2$ (2.32 g/cm^3).

Thus, Eq. A1 can be written in the following modified form

$$\varepsilon_p = \frac{V_{Pore}}{V_{Pore} + (1 - \alpha)V'_{MgO} + \alpha V'_{MgCl_2}} \quad \text{(D7)}$$

where V_{Pore} is the total pore volume per gram of sample after reaction, from Table 5.

The value of the void fraction can be calculated using Eq. D7 and experimental values of pore volume and conversion of MgO to $MgCl_2$. The values of effective diffusivity are calculated from Eq. D4 using the void fraction obtained using Eq. D7. The values of Thiele modulus are then calculated using Eq. D2.

Manuscript received Nov. 6, 2003, and revision received Mar. 18, 2004.